buildings

MDPI

Article

Optimization of the Composition of Cement Pastes Using Combined Additives of Alumoferrites and Gypsum in Order to Increase the Durability of Concrete

Svetlana V. Samchenko, Irina V. Kozlova and Andrey V. Korshunov *

Department of Building Materials, Moscow State University of Civil Engineering, 26, Yaroslavskoye Shosse, 129337 Moscow, Russia
* Correspondence: androkor@mail.ru

Abstract: The reliability of concrete structures is closely related to the durability of the concrete materials stable under external environmental conditions. The present study is aimed at analysing the effect of a prospective hardening additive containing calcium alumoferrites and calcium sulfate (AFCS) as a substitute (5–15%) for Portland cement. The hardened cement pastes were characterized by water absorption, shrinkage, strength and corrosion resistance. It was shown that replacing a part of Portland cement with the AFCS additive results in an increase in the strength of fine-grained concrete and in the water resistance grade of concrete. The use of the AFCS additive in the mixed cements reduces the shrinkage of cement stone, resulting in shrinkage-free fine-grained concretes. The increased corrosion resistance of the hardened cement paste is caused by a chemical (saturation) equilibrium between corrosive medium and a cement stone. Penetration of sulphate ions from corrosive solution into the hardened cement paste is much lower, unlike Portland cement. Following saturation of the hardened cement paste with sulphate ions, their further penetration into the cement stone does not occur. Based on the results of the study, recommendations were developed for the use of the hardening alumoferrite-gypsum additive to Portland cement, which allows to improve the mechanical and corrosion characteristics of concrete.

Keywords: optimized cement paste; combined additive; alumoferrite; gypsum; dense structure; shrinkage; corrosion resistance

Citation: Samchenko, S.V.; Kozlova, I.V.; Korshunov, A.V. Optimization of the Composition of Cement Pastes Using Combined Additives of Alumoferrites and Gypsum in Order to Increase the Durability of Concrete. *Buildings* **2023**, *13*, 565. https://doi.org/10.3390/buildings13020565

Academic Editor: Fuyuan Gong

Received: 20 January 2023
Revised: 15 February 2023
Accepted: 17 February 2023
Published: 19 February 2023

1. Introduction

The modern development of the building industry is associated with the widespread use of concrete. The mostly used construction material is reinforced concrete with the steel reinforcement. Although concrete is an ideal material to protect the steel reinforcement from corrosion damage, the durability of the constructions is also related to the durability of the cementitious materials of which they consist [1–5]. The main chemical causes of concrete destruction are alkali-silica and alkali-carbonate reactions, carbonation, sulfate and chloride exposure, and steel corrosion as well [6–10]. A combination of the mentioned processes leads to substantial deterioration of concrete structures. In addition to the above, acting singly or in combination, a number of factors, such as high structural stresses, thermal stresses, shrinkage, poor material quality and inadequate maintenance can exacerbate the situation [11].

At present, much attention is paid to the problem of corrosion damage of concrete. Researchers are searching for possibilities to increase the resistance of cement compositions using corrosion-resistant binders, aggregates and additives [12–17]. The problem of resistance of concrete materials against the external impacts is especially important when using multicomponent cements [18–22]. Extensive data have been accumulated on the behavior of various cements in corrosive media [6,23]. From the physical point of view, the corrosion process occurs when water or other corrosive medium penetrates into the pores of concrete

causing the material erosion. The resulting effect depends on a material porosity and duration of exposure to corrosive medium [14–16]. From the chemical point of view, the hydration processes occurring when cementitious materials come into contact with water lead to the formation of a number of hydrate compounds [24]. Those compounds, when subjected to the influence of an aggressive medium, undergo transformations which lead to their decomposition, and as a consequence, to the strength and durability reduction of the cement stone [25–30]. Therefore, in order to protect a concrete material from corrosion, it is necessary to choose a binder with components that produce substances stable to the destructive impact of the corrosive medium.

One of the corrosion-resistant cements are those containing sulfate components, there are known studies on corrosion resistance of hardened cement pastes with sulfated cement additives [25,29–33]. To obtain expanding and straining cements, the expanding additives based on sulfated clinkers, produced on the basis of various iron-containing technogenic materials, have recently attracted the special interest of researchers. Sulfoferrite and sulfoaluminoferrite clinkers can be used as components of mixtures with Portland cement (up to 15%) [31,32]. The hydration properties of sulfated clinkers and the composition of hydrated minerals make it possible to create a whole range of cements with specified properties—from expanding to high-strength ones. Moreover, a special role in the formation of the structure of cement stone using such clinkers belongs to ettringite. It is an important component of cement stone, largely determining its strength and deformation properties.

It is known [24] that the sulfate corrosion of concretes is characterized by processes that occur when they are accompanied by the accumulation of poorly soluble reaction products in the pores of concrete. Such substances are capable of increasing the volume of the solid phase in the pores of concrete during phase transitions or polymerization. As a consequence, internal stresses are created in the concrete destroying its structure. The shrinkage deformations arising from corrosion can lead to the formation of cracks and other defects in the structure of building materials, reducing the service life of these materials [34]. Therefore, in order to increase the durability of concrete, a number of additives that reduce or affect shrinkage are introduced into the composition of concrete [34–37].

The sulfate aggression is the most common since sulfate ions are present in almost all types of natural and wastewaters. In the process of the sulfate corrosion of cement stone, gypsum and ettringite are formed according to the following schemes:

$$Ca(OH)_2 + Na_2SO_4 + 2H_2O \rightarrow CaSO_4 \cdot 2H_2O + 2NaOH$$

$$CaSO_4 \cdot 2H_2O + 3CaO \cdot A1_2O_3 \cdot 6H_2O + 24H_2O \rightarrow 3CaO \cdot Al_2O_3\ 3CaSO_4 \cdot 32H_2O$$

The volume occupied by ettringite is 2.27 times larger than the volume of the initial hydration products. At the initial stage of corrosion, the resulting products seal and strengthen the concrete, but then excessive accumulation of reaction products leads to the formation of cracks and to a decrease in the strength of concrete. Despite the fact that the sulfate corrosion of concrete has been the subject of extensive research, some aspects of this complex process are still not clear.

Therefore, studies on the improvement of the corrosion resistance of hardened cement pastes will enrich the scientific knowledge on the formation of the structure of hardened cement paste and will be useful in optimizing the structure of corrosion resistant and durable concretes.

The purpose of the present study was to optimize the composition and structure of the hardened cement pastes using additives of alumoferrites and gypsum in order to increase the resistance against sulphate corrosion.

2. Materials and Methods

2.1. Materials

In the present work, an ordinary Portland cement (OPC) CEM I 42.5 H, in accordance with GOST 31108, was used. The hardening additive (Table 1), consisting of calcium

alumoferrites and calcium sulfate (AFCS), was used to replace a definite share (5, 10 and 15%) of the Portland cement in the pastes to optimize their structure. The characteristics of the additive and cement are presented in Table 1. The samples made of cement without additive served as the control ones. The samples were prepared by the conventional mixing method consisting in introducing a weighed amount of AFCS into the cement and aggregate mixture. A polyfractional sand was used as an aggregate. The mineralogical composition of the materials is presented in Table 2.

Table 1. Characteristics of the hardening alumoferrite-gypsum additive and cement.

	AFCS	**OPC**
SiO_2, %	14.40	22.03
Al_2O_3, %	8.70	5.15
Fe_2O_3, %	16.20	4.86
CaO, %	51.90	65.41
MgO, %	1.17	1.20
SO_3, %	4.60	0.34
Loss of ignition, %	0.01	0.21
Density, m^3/kg	2.90	3.16
Blaine grinding fineness cm^2/g	4230	3190

Table 2. Mineralogical composition of the hardening additive and cement.

	AFCS	**OPC**
Alite	10	67
Belite	25	15
Tricalcium aluminate	-	5
Tetracalcium alumoferrite	65	13

In this work, the sulfate solutions 5% Na_2SO_4 and 1% $MgSO_4$ were used as corrosive media.

2.2. Experimental Procedure

2.2.1. Mixture Proportioning

The cement samples studied were prepared by mixing the weighed amounts of components shown in Table 3. The sample compositions are labeled in "X-Y" format, where X is the OPC content and Y is the AFCS content (%). The water-cement ratio was 0.5 according to EN 196.1.

Table 3. Compositions of the mixed cements (mass, g).

Material	**The Designation of the Composition "X-Y"**			
	100-0	**95-5**	**90-10**	**85-15**
OPC	450	427.5	405	382.5
AFCS	-	22.5	45	67.5
Water	225	225	225	225
Polyfractional sand	1350	1350	1350	1350

2.2.2. Cement Mixing

The cement mixtures were produced using an automatic programmable mixer CONTROLS 65-L0006/AM with planetary rotation of the working body (Figure 1) in two speed modes: slow speed—blade rotation 140 ± 5 rpm, fast speed—blade rotation 285 ± 10 rpm. The sequence of the mixing operations are shown in Table 4. The components were mixed in a plastic drum with rubber balls. The mixing procedure was performed as follows. The sand was poured into the metering device of the mixer. Water was poured into the mixer bowl previously wiped with a damp cloth, and then the pre-mixed cement was added. Following this, the mixer was turned on at low speed and mixed the components. Following this stage of mixing, sand was added and the mixing continued at low speed, after which the cement mortar was additionally mixed.

Figure 1. Automatic programmable mixer 65-L0006/AM.

Table 4. Parameters of the preparation of the cement mixtures.

№	Description of the Procedure	Procedure Duration, min	Mixer Speed Mode
1	Mixing of the components	1.0	Slow
2	Adding water, mixing	1.5	Slow
3	Pause, manual stirring	1.0	-
4	Mixing	2.0	Rapid
5	Mixing	1.5	Slow
Total mixing time, min		7.0	

2.3. Test Procedure

2.3.1. Strength Test

To determine the strength characteristics, the 40 × 40 × 160 mm cement beam samples were prepared using a steel mold. The samples were cured in a normal curing chamber for the first day, and then they were immersed in distilled water for 28 days at 22 °C. Following this period, the samples were removed from the water and further stored under ambient laboratory conditions.

At day 28, the samples were tested on bending and compression in accordance with GOST 30744. The bending test was carried out using a PM-A-70AB press (Figure 2a). The bending strength R_{str} was calculated by Formula (1):

$$R_{str} = \frac{1.5Fl}{b^3} \quad (1)$$

where

F_{str} is the breaking load, N;

b is the size of the side of the square cross-section of the beam sample, mm;

l is the distance between the axes of supports, mm.

The arithmetic mean value of the test results of three samples was taken as the bending strength. The calculation result is rounded to 0.1 MPa.

The compression test was performed on a CONTROLS MCC8 50-C8422 press at a speed of 2.5 MPa/s (Figure 2b). The compressive strength (R_{com}, MPa) was calculated using Formula (2):

$$R_{com} = \frac{F_{com}}{S} \quad (2)$$

where

F_{com} is the breaking load, N;

S is the cross-sectional area, mm^2.

The arithmetic mean value of the results of six tests was taken as the compressive strength of a series of samples.

(**a**) (**b**)

Figure 2. Equipment used to perform the bend (**a**) and compression (**b**) tests.

2.3.2. Water Absorption Test

The water absorption was determined by testing samples in the state of natural humidity according to GOST 12730.3. The three samples for each composition studied were weighed every 24 h of water absorption on hydrostatic scales with an error of no more than 0.1%.

The water absorption for each sample (W_m, wt. %) was calculated with an error of 0.1% by Formula (3):

$$W_m = \frac{m_v - m_c}{m_c} \cdot 100\% \quad (3)$$

where

m_v is the mass of a wet sample, g;

m_c is the mass of a dry sample, g.

2.3.3. Water Permeability Test

Determination of the water permeability was performed in accordance with GOST 12730.5 using the filtration coefficient. The water pressure increase was achieved with 0.2 MPa steps for 1–5 min after 1 h exposure at each step to the pressure, at which the water filtration in the form of individual drops was observed. The values of the filtrate mass and volume were measured every 30 min, six times for each sample. The filtrate volume of an individual sample (Q) is taken as the arithmetic average of the four largest values. The water permeability of concrete was determined by testing a series of six samples.

The filtration coefficient (K_f, cm/s) of an individual sample was determined by Formula (4):

$$K_f = \frac{\eta \cdot Q \cdot \delta}{S \cdot \tau \cdot p} \quad (4)$$

where

η is the water viscosity coefficient (η = 1.00 at 20 °C);
Q is the volume of a filtrate, cm^3;
δ is the thickness of a cement sample, cm;
S is a cement sample area, cm^2;
τ is the test time, s;
p is the pressure in the setup, cm of the water column.

2.3.4. Expansion and Shrinkage Tests

Deformation of the hardened cement mortars was evaluated by testing the 40 × 40 × 160 mm beam specimens. One day after molding, a brass adhesive rod was glued to the center of each end face of the beam sample. A quickly polymerizing non-expanding glue (epoxy resin 80 g, polyethylene polyamine 3 g, dibutyl phthalate 1 g) was used to fasten the adhesive. Prior to testing, an indicator-type device (Figure 3) was adjusted to the samples to measure the strain. Once the length of the samples was measured, they were stored in water. To determine the deformative properties, three beam samples of each composition were made.

Figure 3. Sample strain measurement device.

Deformation of hardened cement specimens was evaluated using Formula (5):

$$\varepsilon_0 = \frac{\Delta L}{L} \cdot 100 \quad (5)$$

where

ε_0 is the total shrinkage, %;
ΔL is the difference between the final and initial references of the indicator, mm;
L is the length of the sample, mm.

2.3.5. Corrosion Resistance Testing

Following the curing of the samples in water for 28 days, some of them were immersed in an aggressive medium for 90, 180 and 360 days; a part of the samples was placed in pure water. Samples cured both in water and in aggressive solutions were tested for residual strength, and their structure was studied as well. The durability coefficient (K_c) was calculated using Formula (6):

$$K_c = \frac{R_{am}}{R_{sc}} \quad (6)$$

where

R_{am} is the ultimate strength of the samples cured in a corrosive medium, MPa;
R_{sc} is the ultimate strength of the samples cured under standard conditions, MPa.

2.3.6. Physical Structure and Chemical Analysis

The physical structure of the hardened cement paste was studied by determining the porosity by an inert liquid saturation and by a low pressure mercury porosimeter, and using scanning electron microscopy (SEM, JEOL JSM-7500F) as well.

Absorption of sulfate ions from the corrosive solution by the solidified samples was determined by a chemical method of analysis according to GOST 5382.

3. Results and Discussion

3.1. The Physical Essence of Optimizing the Structure of Hardened Cement Paste

The physical essence of optimizing the structure of hardened cement paste is based on the controlled formation of a dense structure. A dense structure of the stone is formed due to mutual sprouting of the crystal framework formed by crystalline hydrates of the hardening additive (AFCS) and by the low-crystallized calcium hydrosilicates during the hydration of Portland cement.

Formation of the crystal structure in the studied samples occurs as a result of hydration of the AFCS additive, which contains an increased amount (65%) of calcium alumoferrite. The empirical composition of calcium aluminoferrite can be represented by the formula $C_2A_{1-x}F_x$, where x = 0.5 (the formula can be rewritten as $C_2A_{0.5}F_{0.5}$). Increasing the element ratio Al/Fe up to unity, one can obtain C_4AF. (Here and further in all formulas, the following designations are used: C—CaO; A—Al_2O_3; F—Fe_2O_3).

The hydration of C_4AF in the presence of calcium hydroxide occurs according to reaction (7):

$$C_4AF + Ca(OH)_2 + 14H_2O \rightarrow C_2AH_8 + C_3FH_6 \quad (7)$$

This reaction results in the crystallization of hexagonal crystal hydrates of calcium hydroaluminates of composition C_2AH_8 and of cubic calcium hydroferrites of composition C_3FH_6.

In the presence of calcium sulfate ($CaSO_4$), calcium hydroaluminates C_2AH_8 form ettringite crystals by reaction (8):

$$C_2AH_8 + 3CaSO_4 + Ca(OH)_2 + 23H_2O \rightarrow 3CaO{\cdot}Al_2O_3{\cdot}3CaSO_4{\cdot}32H_2O \quad (8)$$

The presence of calcium hydroxide ($Ca(OH)_2$) is necessary for the reactions (7) and (8) to proceed, resulting in the formation of the crystalline hydrates. Calcium hydroxide is formed in large quantities during the hydration of Portland cement, mainly due to hydrolysis of tricalcium silicate C_3S. It follows from the given reactions that the hardening additive plays a role of a calcium hydroxide binder. Thus, due to the combination of hydrolytic and sulfate consumption processes, formation of a dense structure within the hardened cement samples occurs when a part of Portland cement is substituted by the AFAS additive.

The SEM-images of the obtained hardened structures are shown in Figure 4.

According to the electron microscopy data (Figure 4a), the OPC structure can be characterized as a block-rhythmic structure. Such a structure is formed during the crystallization of $Ca(OH)_2$ in the form of portlandite blocks. The rhythmic structure is caused by the somatic transport of the gel-like mass of calcium hydrosilicates C-S-H to the surface of these blocks. The structure of the hardened samples of mixed cements, as compared to the previous one, has a monotonic character (Figure 4b–d). No large portlandite blocks can be observed because $Ca(OH)_2$ takes part in the formation of the AFt phases. The AFt phases are germinated with calcium hydrosilicates. The formed crystalline hydrates of the AFt phases have a fine-fiber structure, and fill the small pores of the stone. Due to the crystallization of the AFt phases in the pore space, not only the pores are formed as a result

of water binding, but also the air pores (Figure 4c,d). As a result, the cement stone has a lower porosity by 15–23%, both during storage under normal conditions or in various aggressive media. The results of the porosity analysis are shown in Figures 5–7.

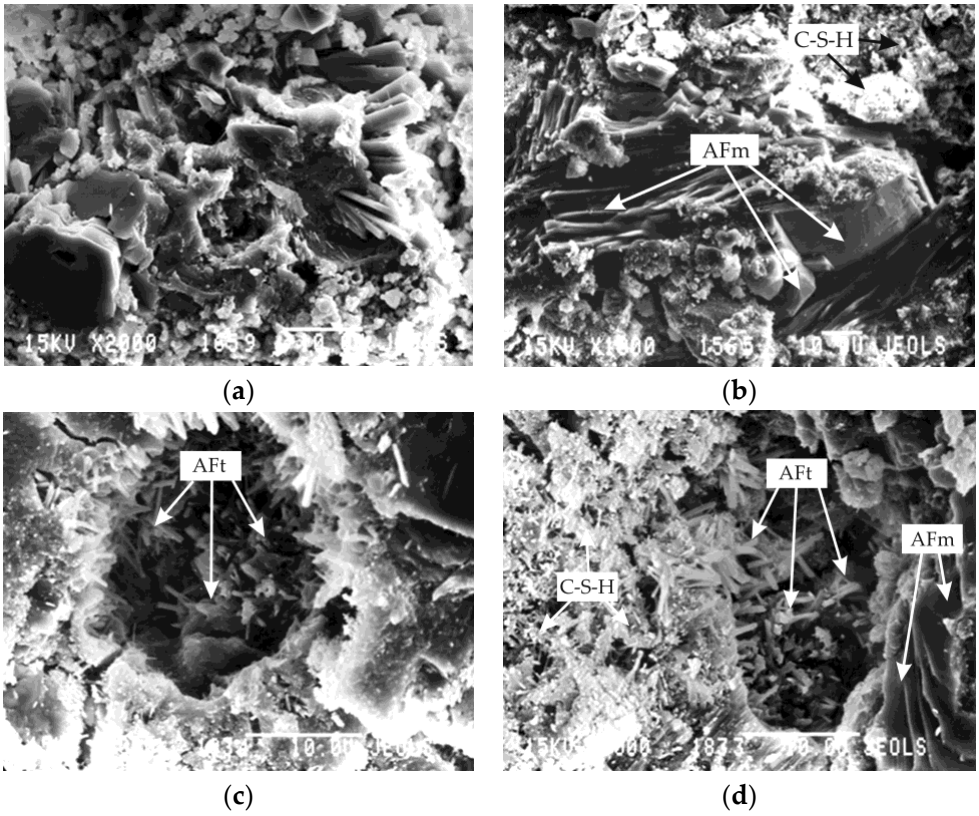

Figure 4. SEM-images of the structure of hardened cement samples kept in water for 28 days; (**a**) sample 100-0; (**b**) sample 95-5; (**c**) sample 90-10; (**d**) sample 85-15.

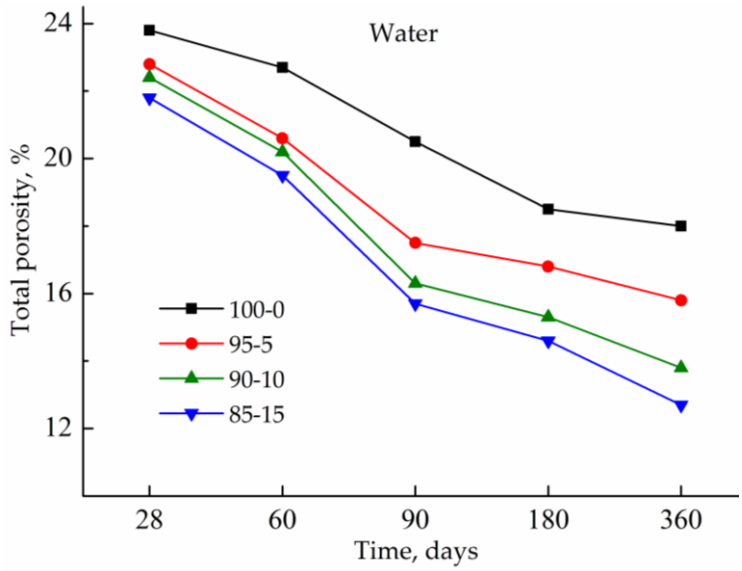

Figure 5. Total porosity of the mixed cement samples hardened in water.

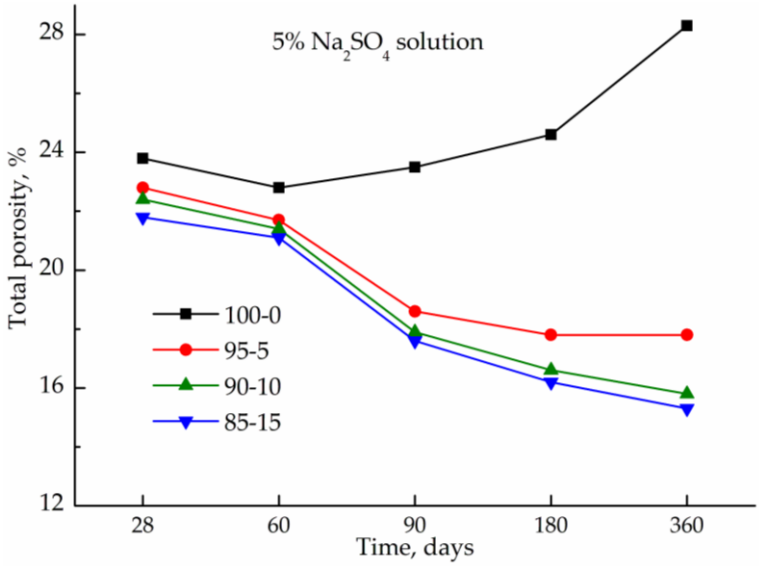

Figure 6. Total porosity of the mixed cement specimens hardened in 5% Na_2SO_4 solution.

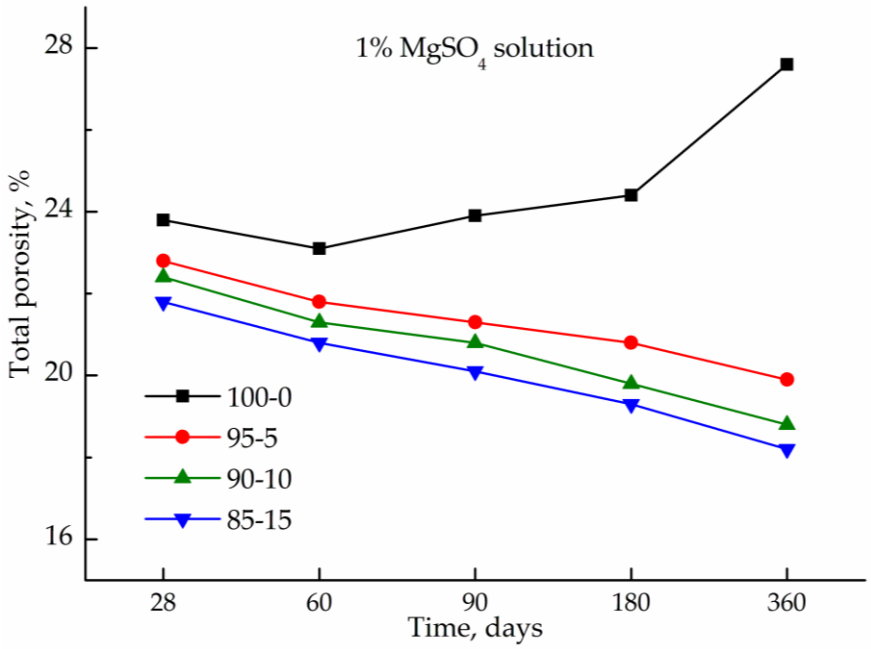

Figure 7. Total porosity of the mixed cement specimens hardened in 1% $MgSO_4$ solution.

Optimizing the structure of the hardened cement paste by replacing a part of the Portland cement leads to an increase in the density of the samples. The values of the density of the samples of different composition are shown in Figure 8. As can be seen from the presented results, the higher the AFCS additive content, the lower the porosity of the samples, and the higher the density. Such a density structure with reduced porosity is observed in samples with higher strength and with lower water absorption. The strength of the mixed cement samples cured under normal conditions is presented in Table 5.

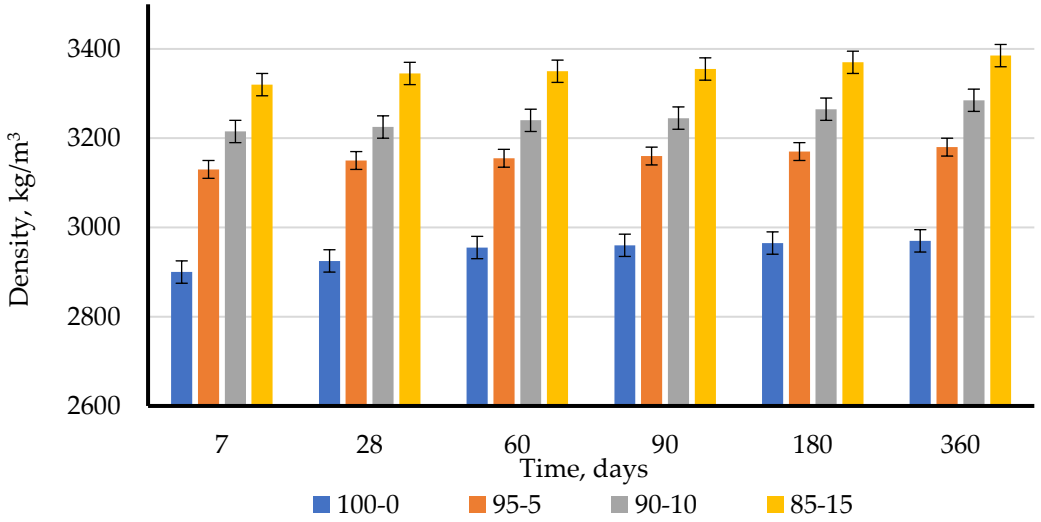

Figure 8. Density of the mixed cement samples at different periods of hardening.

Table 5. Results of the strength tests of the cement samples at different periods of hardening (days).

Sample	Flexural Strength, MPa					Compressive Strength, MPa				
	28	**60**	**90**	**180**	**360**	**28**	**60**	**90**	**180**	**360**
100-0	6.8	8.8	9.8	11.1	12.3	49.4	54.2	56.9	58.7	59.2
95-5	6.1	8.6	10.0	11.4	12.5	47.3	53.8	58.1	60.4	62.6
90-10	5.9	9.3	11.2	12.4	13.1	46.5	53.2	58.8	61.7	63.6
85-15	5.3	8.8	10.6	12.0	12.6	45.2	51.8	57.1	60.1	62.0

As can be seen from Table 5, the compressive and tensile strength of the fine-grained concrete samples decreases as the AFCS content increases at the early stages (7 and 28 days). At the same time, expansion of the specimens also takes place. Later, after three months, the highest compressive strength is achieved for the 10% AFCS samples without their shrinkage. The increased amount of formed AFt phase crystallohydrates (Figure 4) leads to the expansion of the hardening structure, which is accompanied by a decrease in the compressive strength of the samples by 4.25–8.50% (after 28 days). By 360 days, the strength of the samples, on the contrary, increases by 4.7–7.4%. The observed effects can be explained by the accumulation of calcium hydrosilicate submicrocrystals in the intercrystalline space of the crystal framework of AFt phases.

The results of the determination of water absorption are presented in Table 6. The increased strength and density of the cement matrix when replacing a part of Portland cement with the AFCS additive makes it possible to obtain a hardened cement paste with a reduced filtration coefficient by 2.6–2.1 times for compositions 95-5 and 85-15, and by 4.6 times for compositions 90-10, as compared to the Portland cement sample. Thus, using the alumoferrite-gypsum additive allows to increase the strength of fine-grained concrete as well as the grade of concrete for water resistance (from W8 to W14).

The results of the determination of the mixed cement samples expansion (shrinkage) are shown in Figure 9. As can be seen from the data obtained, the Portland cement samples undergo shrinkage. The mixed cement samples show no shrinkage, but expansion occurs during the first 14 days of hardening. Such an effect can be explained by the formation of a crystalline structure in the hardening cement paste. When the crystallization is completed, the caged structure fills in with fine crystals of calcium hydrosilicates. During this period, the expansion process is stabilized, and the strength (density) of the samples increases.

Table 6. Permeability of the mixed cement samples.

Sample	Filtration Coefficient, K_f cm/s	Water Absorption, wt. %	Water Resistance Grade
100-0	$5.5 \cdot 10^{-10}$	4.1	W8
95-5	$2.6 \cdot 10^{-10}$	3.5	W12
90-10	$1.2 \cdot 10^{-10}$	2.9	W14
85-15	$2.1 \cdot 10^{-10}$	3.2	W14

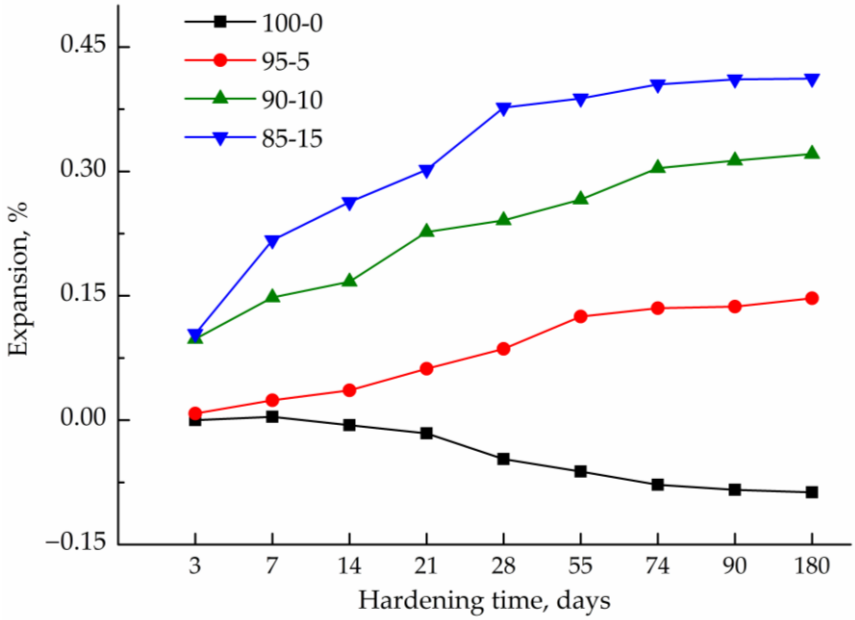

Figure 9. Expansion (shrinkage) of the mixed cement samples during different hardening periods.

The analysis of the data presented above allows us to conclude that the substitution of a part of Portland cement with the AFCS additive makes it possible to optimize the structure of the hardened cement paste. Optimization of the structure is based on the controlled formation of a dense strong structure. This leads to an increase in the strength of fine-grained concrete and to an increase in the water resistance grade of concrete. Moreover, the AFCS additive makes it possible to control the expansion (shrinkage) of the samples.

3.2. Chemical Essence of the Increased Corrosion Resistance of Hardened Cement Paste

The chemical essence of the increased corrosion resistance of the hardened cement paste consists in the affinity of the chemical and mineral structures of the components of the AFCS additive to Portland cement.

Formation of a tough dense structure of the hardened cement paste causes an increase in its corrosion resistance. The kinetics of a change in the resistance coefficients for the mixed cement samples is shown in Figures 10 and 11. The resistance coefficient of the mixed cements exceeds the unity which indicates an increase in their strength during hardening in aggressive media, in contrast to OPC, in which the resistance coefficient gradually decreases. The higher corrosion resistance is achieved by establishing a chemical equilibrium between the corrosive medium and the hardened cement paste: the hardened cement paste contains crystalline hydrates with ions identical to those of the corrosive medium. The AFCS additive also contains sulfate ions (Table 1).

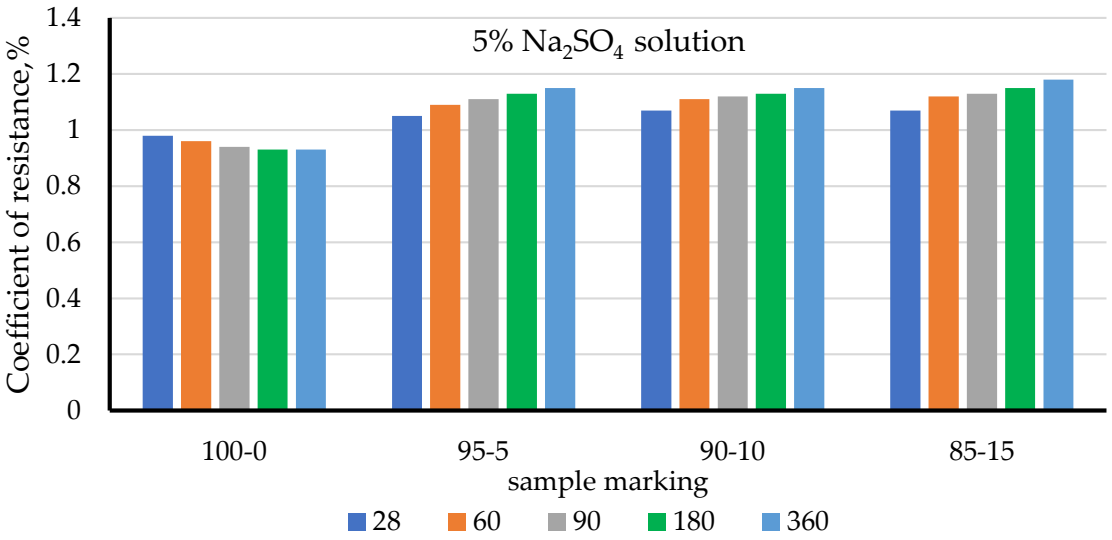

Figure 10. The coefficients of corrosion resistance of the mixed cement samples during different periods (days) of hardening in 5% Na_2SO_4 solution.

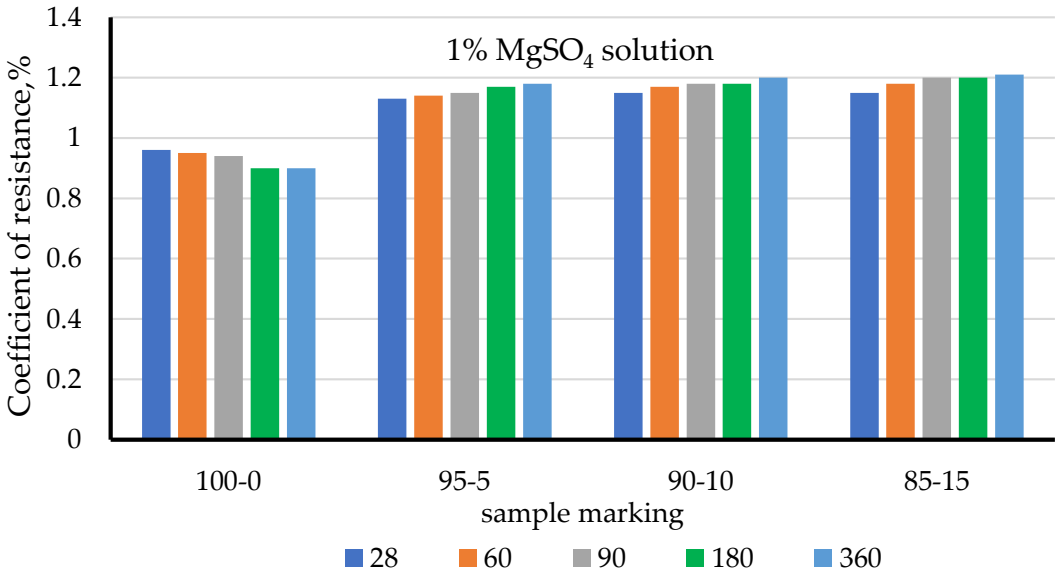

Figure 11. The coefficients of corrosion resistance of the mixed cement samples during different periods (days) of hardening in 1% $MgSO_4$ solution.

The results of absorption measurements (Figures 12 and 13) show that the hardened cement paste does not absorb sulphate ions from the solutions during the first 14 days, in contrast to Portland cement. A slightly increased absorption of sulphate ions by the mixed cements is observed only by day 28 of hardening, and further substantial penetration of sulphate ions into the cement stone does not occur. Such a resistance to the sulphate attack can be explained by establishing a saturation equilibrium between the corrosive medium and the cement stone.

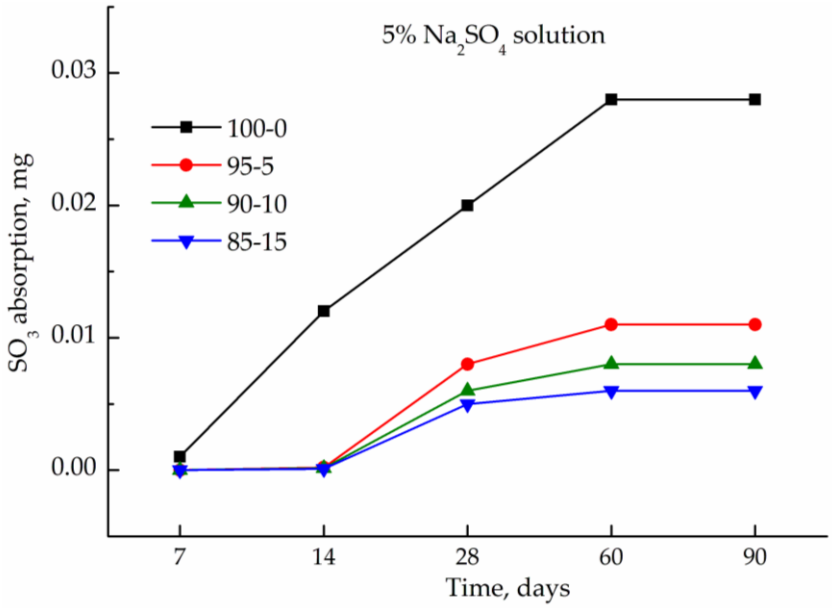

Figure 12. Kinetics of the sulphate ions absorption by the mixed cement samples from 5% Na_2SO_4 solution.

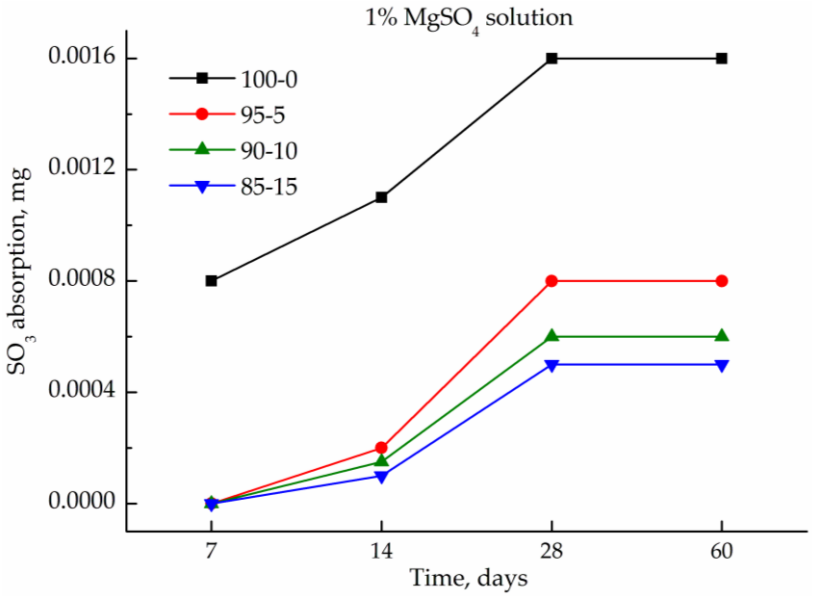

Figure 13. Kinetics of the sulphate ions absorption by the mixed cement samples from 1% $MgSO_4$ solution.

In turn, the achieved equilibrium at substantially lower absorbed sulphate contents is determined by the dense structure of the hardened cement paste formed by crystalline hydrates of AFt phases densified with a gel-like mass of calcium hydrosilicates C-S-H. The hardened cement paste consists of hydrate phases which contain sulphate ions identical to ions in the corrosive media. This results in the absence of the concentration gradient between solid and liquid phases, and therefore, in lower corrosion damage by sulphate solutions. It is also necessary to note that the structure of the hardened cement paste must be formed with AFt phases and must exclude AFm phases which are the most sensitive to the sulphate corrosion. Exposure to the corrosive sulphate solutions leads to complete decomposition of AFm phases within the stone structure followed by crystallization of AFt phases. This transformation is accompanied with calcium leaching from the structural components of the hardened cement paste and results in its destruction.

4. Conclusions

1. The physical essence of optimizing the structure of the hardened cement paste is based on the controlled formation of a dense structure. The hydrated OPC structure is characterized by block-periodic structure and is formed by $Ca(OH)_2$ blocks and by non-hydrated grains covered with a gel-like mass of calcium hydrosilicates C-S-H. The OPC stone has an open porosity of about 23% after 90 days of curing in water. During storage in sulphate solutions, porosity increases due to dissolution and leaching of $Ca(OH)_2$. At the same time, the coefficient of corrosion resistance of the OPC stone in the corrosive environments decreases;

2. The structure of the mixed cements, containing the hardening alumoferrite-gypsum (AFCS) additive and cured in water, is formed by AFt crystalline hydrates with a gel-like mass of calcium hydrosilicates C-S-H. The samples are characterized by an open-type porosity of 16% after 90 days. When stored in sulphate solutions, porosity decreases due to crystallization of AFt faces resistant to subsequent dissolution. In such cements, not only pores formed as a result of water binding, but also air pores become overgrown. As a result, the cement stone had a 15–23% lower porosity, both during storage under normal conditions as well as in various corrosive solutions. Replacing a part of the Portland cement with the AFCS additive results in an increase in the strength of fine-grained concrete and in an increase in the water resistance grade of concrete. The use of the AFCS additive in mixed cements reduces the shrinkage of cement stone, resulting in shrinkage-free fine-grained concretes. At the early stages (7 and 28 days), the compressive and tensile strength of the cured cement paste decreases as the AFCS content increases;

3. The chemical essence of increased corrosion resistance of the hardened cement paste consists in the formation of affinity structures, and the chemical and mineralogical nature is analogous for the both AFCS additive and Portland cement. From the chemical point of view, the increased corrosion resistance of the hardened cement paste is caused by a chemical (saturation) equilibrium between the corrosive medium and a cement stone. The hydrate phases in the hardened cement contain sulphate ions identical to those in the corrosive solutions. Penetration of sulfate ions from the corrosive solution into the hardened cement paste is much lower unlike Portland cement. Following saturation of the hardened cement paste with sulphate ions, their further penetration into the cement stone does not occur;

4. The structure of the hardened cement paste should be formed with the participation of AFt phases which are stable against the sulphate corrosion. Exposure of AFm phases to sulphate containing media leads to the complete decomposition of the stone structure with subsequent crystallization of the AFt phases. This transformation is accompanied with calcium leaching from the hardened cement paste and leads to its destruction;

5. The practical use of the alumoferrite-gypsum additive can be effective in replacing sulfoaluminate cement. The Portland cement mixtures with the additive have normal setting times, provide good rheological properties of cement mortars and high corrosion resistance. The hardened cement compositions can be used to obtain the waterproof high-strength concrete with compensated shrinkage for hydraulic engineering constructions.

5. Possible Directions for Future Studies

To optimize the structure and properties of the hardened cement paste containing alumoferrite-gypsum additive, it is necessary to continue research to establish the effect of various surfactants on the morphology of the resulting crystallohydrates.

Author Contributions: Conceptualization, S.V.S., I.V.K. and A.V.K.; methodology, S.V.S.; software, I.V.K. and A.V.K.; validation, S.V.S., I.V.K. and A.V.K.; formal analysis, S.V.S., I.V.K. and A.V.K.; investigation, S.V.S., I.V.K. and A.V.K.; resources, S.V.S., I.V.K. and A.V.K.; data curation, S.V.S., I.V.K. and A.V.K.; writing—original draft preparation, S.V.S., I.V.K. and A.V.K.; writing—review and editing, S.V.S.; visualization, S.V.S., I.V.K. and A.V.K.; supervision, S.V.S.; project administration, S.V.S.; funding acquisition, S.V.S., I.V.K. and A.V.K. All authors have read and agreed to the published version of the manuscript.

Funding: The research was carried out with the financial support of Moscow State University of Civil Engineering.

Institutional Review Board Statement: Not applicable.

Informed Consent Statement: Not applicable.

Data Availability Statement: The data presented in this study are available upon request from the corresponding author.

Conflicts of Interest: The authors declare no conflict of interest.

References

1. Maruyama, I.; Rymeš, J.; Aili, A.; Sawada, S.; Kontani, O.; Ueda, S.; Shimamoto, R. Long-term use of modern Portland cement concrete: The impact of Al-tobermorite formation. *Cem. Concr. Res.* **2014**, *58*, 20–34. [CrossRef]
2. Pishro, A.A.; Feng, X.; Ping, Y.; Dengshi, H.; Shirazinejad, R.S. Comprehensive equation of local bond stress between UHPC and reinforcing steel bars. *Constr. Build. Mater.* **2020**, *262*, 119942. [CrossRef]
3. Loreto, G.; Benedetti, M.D.; Luca, A.D.; Nanni, A. Assessment of reinforced concrete structures in marine environment: A case study. *Corros. Rev.* **2019**, *37*, 57–69. [CrossRef]
4. Srividhya, S.; Vidjeapriya, R.; Neelamegam, M. Enhancing the performance of hyposludge concrete beams using basalt fiber and latex under cyclic loading. *Comput. Concr.* **2021**, *28*, 93–105.
5. Prakash, R.; Sudharshan, N.; Subramanian, R.C.; Divyah, N. Eco-friendly fiber-reinforced concretes. In *Handbook of Sustainable Concrete and Industrial Waste Management, Colangelo, F., Cioffi, R., Farina, I., Eds.*; Woodhead Publishing: New York, NY, USA, 2022; pp. 109–145.
6. Aguirre-Guerrero, A.; Mejía-de-Gutiérrez, R.; Montês-Correia, M.J.R. Corrosion performance of blended concretes exposed to different aggressive environments. *Constr. Build. Mater.* **2016**, *121*, 704–716. [CrossRef]
7. Babaee, M.; Castel, A. Chloride-induced corrosion of reinforcement in low-calcium fly ash-based geopolymer concrete. *Cem. Concr. Res.* **2016**, *88*, 96–107. [CrossRef]
8. Ghanooni-Bagha, M.; Shayanfar, M.; Shirzadi-Javid, A.; Ziaadiny, H. Corrosion-induced reduction in compressive strength of self-compacting concretes containing mineral admixtures. *Constr. Build. Mater.* **2016**, *113*, 221–228. [CrossRef]
9. Scott, A.; Alexander, M.G. Effect of supplementary cementitious materials (binder type) on the pore solution chemistry and the corrosion of steel in alkaline environments. *Cem. Concr. Res.* **2016**, *89*, 45–55. [CrossRef]
10. Jiang, L.; Niu, D. Study of deterioration of concrete exposed to different types of sulfate solutions under drying-wetting cycles. *Constr. Build. Mater.* **2016**, *117*, 88–98. [CrossRef]
11. Andrade, C. Future trends in research on reinforcement corrosion. In *Corrosion of Steel in Concrete Structures*; Poursaee, A., Ed.; Woodhead Publishing: New York, NY, USA, 2016; pp. 269–288.
12. Duan, P.; Yan, C.; Zhou, W. Influence of partial replacement of fly ash by metakaolin on mechanical properties and microstructure of fly ash geopolymer paste exposed to sulfate attack. *Ceram. Int.* **2016**, *42*, 3504–3517. [CrossRef]
13. Karakoç, M.B.; Türkmen, İ.; Maraş, M.M.; Kantarci, F.; Demirboğa, R. Sulfate resistance of ferrochrome slag based geopolymer concrete. *Ceram. Int.* **2016**, *42*, 1254–1260. [CrossRef]
14. Shi, Z.; Lothenbach, B.; Geiker, M.R.; Kaufmann, J.; Skibsted, J. Experimental studies and thermodynamic modeling of the carbonation of Portland cement, metakaolin and limestone mortars. *Cem. Concr. Res.* **2016**, *88*, 60–72. [CrossRef]
15. Nadeem, A.; Memon, S.A.; Lo, T.Y. Mechanical performance, durability, qualitative and quantitative analysis of microstructure of fly ash and Metakaolin concrete at elevated temperatures. *Constr. Build. Mater.* **2013**, *38*, 338–347. [CrossRef]
16. Yan, P.; Mi, G.; Wang, Q. A comparison of early hydration properties of cement-steel slag binder and cement-limestone powder binder. *J. Therm. Anal. Calorim.* **2014**, *115*, 193–200. [CrossRef]
17. Berra, M.; Carassiti, F.; Mangialardi, T.; Paolini, A.E.; Sebastiani, M. Effects of nanosilica addition on workability and compressive strength of Portland cement pastes. *Constr. Build. Mater.* **2012**, *35*, 666–675. [CrossRef]
18. Bai, J. Durability of sustainable construction materials. In *Sustainability of Construction Materials*, 2nd ed.; Khatib, J.M., Ed.; Woodhead Publishing: New York, NY, USA, 2016; pp. 397–414.
19. Shehata, M.H.; Adhikari, G.; Radomski, S. Long-term durability of blended cement against sulfate attack. *ACI Mater. J.* **2008**, *105*, 594–602.
20. Ghafoori, N.; Batilov, I.; Najimi, M.; Sharbaf, M.R. Sodium sulfate resistance of mortars containing combined nanosilica and microsilica. *J. Mater. Civ. Eng.* **2018**, *30*, 04018135. [CrossRef]
21. Irassar, E.F. Sulfate attack on cementitious materials containing limestone filler—A review. *Cem. Concr. Res.* **2009**, *39*, 241–254. [CrossRef]
22. Tobón, J.I.; Payá, J.; Restrepo, O.J. Study of durability of Portland cement mortars blended with silica nanoparticles. *Constr. Build. Mater.* **2015**, *80*, 92–97. [CrossRef]
23. Hongke, P.; Zisheng, Y.; Fuwei, X. Study on concrete structure's durability considering the interaction of multi-factors. *Constr. Build. Mater.* **2016**, *118*, 256–261.
24. Taylor, H.F.W. (Ed.) *The Chemistry of Cements*; Academic Press: London, UK; New York, NY, USA, 1964; Volume 1&2.

25. Samchenko, S.; Zemskova, O.; Zorin, D. Corrosion resistance of sulfated cements in carbonate and in carbonate-sulfate mediums. *MATEC Web Conf.* **2017**, *106*, 03014. [CrossRef]
26. Hou, P.; Zhang, R.; Cai, Y.; Cheng, X.; Shah, S.P. In situ $Ca(OH)_2$ consumption of TEOS on the surface of hardened cement-based materials and its improving effects on the Ca-leaching and sulfate-attack resistivity. *Constr. Build. Mater.* **2016**, *113*, 890–896. [CrossRef]
27. Gollop, R.S.; Taylor, H.F.W. Microstructural and microanalytical studies of sulfate attack. II. Sulfate-resisting Portland cement: Ferrite composition and hydration chemistry. *Cem. Concr. Res.* **1994**, *24*, 1347–1358. [CrossRef]
28. Leklou, N.; Aubert, J.-E.; Escadeillas, G. Microscopic observations of samples affected by delayed ettringine formation. *Mater. Struct.* **2009**, *42*, 1369–1378. [CrossRef]
29. Samchenko, S.V.; Kouznetsova, T.V. Resistance of the calcium sulphoaluminate phases to carbonation. *Cem. Wapno Beton* **2014**, *5*, 317–322.
30. Kouznetsova, T.V.; Samchenko, S.V.; Lutikova, T.A. Carbonation of the constituents of hydrated Portland cement, aluminate and sulphoaluminate cements. In Proceedings of the 13th International Baustofftagung—Ibausil, Weimar, Bundesrepublik Deutschland, 24–27 September 1997.
31. Krivoborodov, Y.R.; Samchenko, S.V. Structure formation of cement paste at hydration of sulphoferrite cements. In Proceedings of the 12th International Congress on the Chemistry of Cement (ICCC), Montreal, Canada, 8–13 July 2007.
32. Samchenko, S.V.; Zorin, D.A. Use sulfoferritic cements in construction. *E3S Web Conf.* **2018**, *33*, 02070. [CrossRef]
33. Clarke, C. Concrete shrinkage prediction using maturity and activation energy. Master's Thesis, The Graduated School of the University of Maryland, College Park, MD, USA, 2009.
34. Jones, C. Effect of lightweight aggregate moisture content on internally cured concrete. Bachelor's Thesis, University of Arkansas, Fayetteville, NC, USA, 2013.
35. Mora-Ruacho, J.; Gettu, R.; Aguado, A. Influence of shrinkage reducing admixtures on the reduction of plastic shrinkage cracking in concrete. *Cem. Concr. Res.* **2009**, *39*, 141–146. [CrossRef]
36. Mo, L.; Deng, M.; Wang, A. Effects of MgO based expansive additive on compensating the shrinkage of cement paste under non wet curing conditions. *Cem. Concr. Compos.* **2012**, *34*, 377–383. [CrossRef]
37. Duvallet, T.; Zhou, Y.; Henke, K.R.; Robl, T.L.; Andrews, R. Effects of ferrite concentration on synthesis, hydration and mechanical properties of alite-calcium sulfoaluminate-ferrite cements. *J. Sustain. Cem.-Based Mater.* **2017**, *6*, 85–110. [CrossRef]